

Crystallization and Grain Growth Kinetics for Precipitation-Based Ceramics: A Case Study on Amorphous Ceria Thin Films from Spray Pyrolysis

By Jennifer L. M. Rupp,* Barbara Scherrer, Ashley S. Harvey, and Ludwig J. Gauckler

The introductory part reviews the impact of thin film fabrication, precipitation versus vacuum-based methods, on the initial defect state of the material and microstructure evolution to amorphous, biphasic amorphous-nanocrystalline, and fully nanocrystalline metal oxides. In this study, general rules for the kinetics of nucleation, crystallization, and grain growth of a pure single-phase metal oxide thin film made by a precipitation-based technique from a precursor with one single organic solvent are discussed. For this a complete case study on the isothermal and non-isothermal microstructure evolution of dense amorphous ceria thin films fabricated by spray pyrolysis is conducted. A general model is established and comparison of these thin film microstructure evolution to kinetics of classical glass-ceramics or metallic glasses is presented. Knowledge on thermal microstructure evolution of originally amorphous precipitation-based metal oxide thin films allows for their introduction and distinctive microstructure engineering in devices-based on microelectromechanical (MEMS) technology such as solar cells, capacitors, sensors, micro-solid oxide fuel cells, or oxygen separation membranes on Si-chips.

ordered crystalline structures by subsequent annealing. Due to this special film nature, a unique situation is offered to study dense and compact ceramic bodies over the whole range of microstructure evolution from amorphous to fully nanocrystalline. Conventional ceramic processing hardly allows for such fundamental studies as dense and fully ceramic bodies with grains above 100 nm result after calcination and sintering of the original metal oxide powders. Knowledge of crystallization and its impact on the evolution of amorphous to fully nanocrystalline metal oxide microstructures, as well as on its grain growth kinetics is highly limited and experiments on kinetics are scarce.

It is known that frequently used organic solvents lead to large incorporations of metastable compounds as hydroxyl or carboxyl groups in metal oxides, influencing heavily the crystallization processes of these metal oxides. Therefore, it is most likely that the selected precursor system of an aqueous

1. Introduction

Today's technologies to prepare nanocrystalline metal oxide thin films can be separated into two major areas: i) plasma-based techniques depositing from sintered ceramic pellet targets such as pulsed laser deposition or sputtering,^[1] and ii) precipitation techniques based on aqueous or organic precursors such as spray pyrolysis, sol-gel, spin coating, or chemical vapor deposition.^[2,3] The major difference between both classes of thin film processing is the ability to order atoms at deposition. Whereas mostly crystalline films are deposited in case of the plasma-based thin film methods, purely amorphous films are deposited for the precipitation thin film techniques. These dense amorphous films exhibit a high degree of disorder (microstrain) and can be transformed to

or organic precipitation-based metal oxide thin film affects also its crystallization kinetics. Gorbitz and Hersleth classified up to 50 main solvent groups for metallorganic structures capable of affecting crystallization processes and pointed out that the effect of solvent inclusions in the crystal structures is on their disorder.^[4] Van der Sluis and Kroon categorized three different functions of solvents in metal oxides: as participants in hydrogen bonding networks, as space fillers, and as ligands for completing the coordination around a metal ion.^[5] The molecule length of the solvent affects the ordering of the metal oxide structure. Moreover, it is emphasized by the authors that understanding the solvent-solute interaction is needed to understand and modify crystallization processes of growing crystals in a metal oxide.^[6]

The effect of organic precursors on the formation of amorphous metal oxides and their crystallization is normally studied using traditional chemical powder processing routes, i.e., hydrothermal synthesis, sol-gel, co-precipitation, and spray pyrolysis. The crystallization of amorphous ceria- and zirconia-based particles during calcinations was reported to be strongly dependent on the organic and aqueous content of the original chemical processing. The crystal growth rates of as-deposited ceria powders from

[*] J. L. M. Rupp, B. Scherrer, A. S. Harvey, L. J. Gauckler
Department of Materials, ETH Zurich
ETH Zurich Wolfgang-Pauli-Str.10, Zurich CH-8093 (Switzerland)
E-mail: jennifer.rupp@mat.ethz.ch

DOI: 10.1002/adfm.200900255

polymeric precursor solutions decreased due to high carbon contents compared to powders prepared from aqueous solutions.^[7] In case of sol-gel derived ceria particles a large impact of the hydroxyl groups on the existence of Ce–O–C bonds and the final crystallite size of the powder was confirmed.^[8] Precursors were reported to affect the crystallization enthalpy of doped-zirconia powders for powder processing methods.^[9,10] Large differences in the starting temperature of crystallization ranging from 300 to 450 °C were measured for zirconia-based powders dependent on their chemical processing route.^[11–14] The large discrepancy in crystallization starting temperature was related to the organics chosen for powder processing. The crystallization enthalpy of zirconia particles varied up to 50% dependent on residual bound water present after the gel process.^[15] From literature, it can be concluded that singular findings for the impact of chemical processing on crystallites of ceria and zirconia powders exist, but quantified crystallization studies on the kinetics for the development of amorphous to nanocrystalline microstructures are still lacking. In addition, the impact of crystallization on grain growth kinetics for amorphous metal oxides is still unexplored. One major problem in such studies is to quantify the microstructures and to eliminate their influence on the kinetics of crystallization. Therefore the dense amorphous spray pyrolysis thin films are ideal to learn about crystallization kinetics and their impact on grain growth in general, as well as the role of organics. Earlier investigations on spray pyrolysis ceria-based thin films revealed the presence of carbon residues up to temperatures of 1000 °C.^[16] These residues originated clearly from the organic precursors involved in preparation. In addition, high amounts of amorphous phases were found although grain growth was clearly activated.^[17] Both, the remaining amorphous phase and the chemical residues from precursors resulted in low crystal packaging densities and unusual grain growth kinetics compared to fully microcrystalline material.^[18] Stable microstructures were established after short dwell times in isothermal hold experiments following self-limited grain growth kinetics at low to intermediate temperatures. The indication that an amorphous phase and chemical residues were still present although grain growth was clearly active led to the conclusion that crystallization processes might occur in parallel and affect the grain growth kinetics. Common parabolic grain growth kinetics as in microcrystalline ceramics was only found for annealing of ceria-based spray pyrolysis films at high temperatures.

The electrical conductivity and thermodynamic stability of organic precursor-based ceria-based films also showed a strong dependence on the degree of crystallinity, grain size and organic residue content for the electrical conductivity, and its activation energy, as well as the oxygen partial pressure dependence of the electrolytic domain boundary.^[19–24] In view of the broad field of applications for zirconia and ceria-based ceramics such as gas sensor materials,^[25–28] electrolyte, and anode materials for micro-solid oxide fuel cell membranes,^[22,24,29–34] oxygen pumps, and catalytic supports for automotive exhaust^[35–37] or even biological systems^[38] this is problematic. For one metal oxide material the thin film properties vary strongly depending on the ambient state of crystallization and grain growth, and original content of organics and hydroxyl-groups after preparation. Thus, it is of great interest to gain a fundamental understanding of crystallization and grain growth kinetics in these oxides ranging from amorphous to

biphasic amorphous-nanocrystalline or fully nanocrystalline microstructures.

For the present paper, a simple metal oxide system with only one kind of cation was selected to be deposited in the amorphous state by the organic precursor-based route of spray pyrolysis. As a metal oxide, pure ceria, was chosen which once crystallized remains stable in the cubic fluorite structure from room temperature up to its melting point.^[39] The organic precursor contained its nitrate salt and only one organic solvent, tetraethylene glycol, characterized by a high boiling point, and long molecule length. The idea of these experiments was to investigate fundamentally the isothermal and non-isothermal crystallization and grain growth kinetics for a pure metal oxide system derived from a precursor with one single organic solvent. On the basis of these experimental results a model of crystallization and grain growth and microstructural development from amorphous to biphasic amorphous-nanocrystalline and fully nanocrystalline for metal oxides is sought.

2. Results and Discussions

2.1. Microstructures of CeO₂ Spray Pyrolysis Thin Films

The SEM top-views and cross-sections of the spray pyrolysis CeO₂ thin films on sapphire substrates after non-isothermal heating to 1000 °C with ± 3 °C min⁻¹ are displayed in Figure 1. The films exhibit dense, pore-, and crack-free microstructures with typical film thicknesses around 300 ± 30 nm. Local variations in the film thicknesses result from the statistical distribution of droplets arriving on the substrate.^[3] The low magnification plane-view shows such light and dark shaded regions due to local thickness differences in Figure 1a. Higher magnifications of the in-plane microstructures show the grains with globular shape connected by straight grain boundaries as depicted in Figure 1b–c. Isotropic and dense microstructures can also be confirmed by the cross-section of the film shown in Figure 1d. EDX analysis revealed the presence of pure ceria for all thin films investigated here.

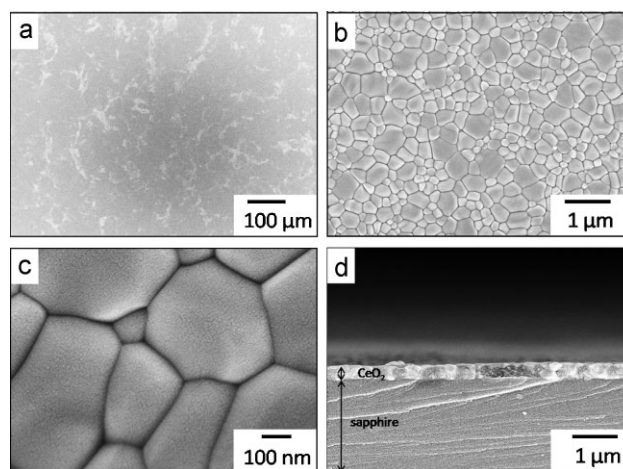


Figure 1. SEM micrographs of spray pyrolysis CeO₂ thin film on sapphire substrate: a–c) top-views and d) cross-section. Thin film is shown after non-isothermal dwell at 1000 °C with ± 3 °C min⁻¹ heating and cooling rate.

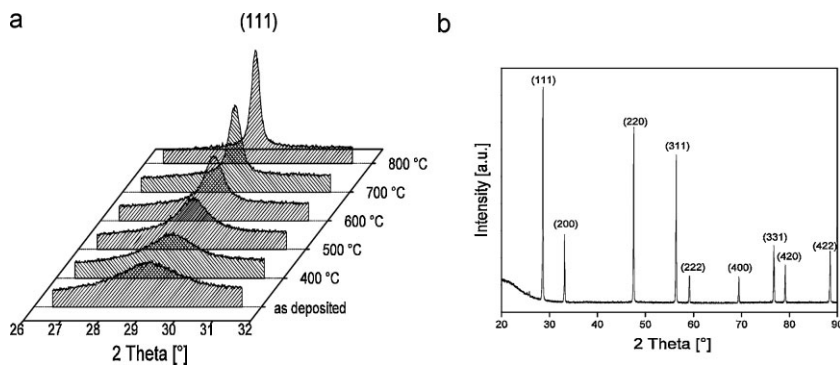


Figure 2. XRD patterns of spray pyrolysis CeO₂ thin film on sapphire substrate: a) Non-isothermal evolution of the (111) peak with $\pm 6^\circ\text{C min}^{-1}$ of an originally as-deposited film and b) overview and peak identification of thin film dwelled without isothermal hold at 900°C with $\pm 3^\circ\text{C min}^{-1}$.

The impact of the non-isothermal heat treatment on the microstructure of an as-deposited CeO₂ spray pyrolysis thin film was monitored using the (111) Bragg peak in an in situ XRD experiment at 6°C min^{-1} heating rate as shown in Figure 2a. The as-deposited film exhibits a broad halo, which develops to a distinctive peak with increasing temperature. This confirms the original amorphous nature of the as-deposited film, and its ability to crystallize upon heating. The XRD pattern of an annealed film at $900^\circ\text{C} \pm 3^\circ\text{C min}^{-1}$ without an isothermal hold revealed sharp XRD reflections in accordance with the cubic fluorite crystal structure of CeO₂^[39,40] as is shown in Figure 2b.

Crystal lattice constants and crystallographic density as determined from XRD patterns during in situ heating (Fig. 1a) are summarized in Table 1. It is remarkable that while increasing temperature from room temperature to 800°C the lattice constant strongly decreases from 0.577 to 0.548 nm. Consequently the crystallographic density increases from 5.940 to 6.915 g cm⁻³ (-14.1%). Progressing crystallization of the CeO₂ films leads to periodic ordering of its atoms, and an increase of the overall lattice packaging density. Even after annealing at 800°C the lattice constant of 0.548 nm is close but still larger than that of state-of-the-art sol-gel derived CeO₂ powders around 0.541 nm.^[8]

Qualitatively similar findings were reported in the case of annealed CeO₂ nanoparticles produced via a soft chemistry route.^[41] For these particles the lattice constant decreased from 0.5417 to 0.5410 nm while temperature was increased from 300 to

Table 1. Lattice constant and crystallographic density for CeO₂ spray pyrolysis thin films as determined from in-situ XRD with $\pm 6^\circ\text{C min}^{-1}$ heating rate. According XRD patterns of the (111) Bragg peak are displayed in Figure 2a.

Temperature [°C]	Lattice constant [nm]	Density [g cm ⁻³]
20	0.577	5.940
400	0.569	6.175
500	0.565	6.333
600	0.558	6.579
700	0.553	6.744
800	0.548	6.915

1000°C . This corresponds to a small change in lattice constant around 0.2% for $\Delta T = 700^\circ\text{C}$. In the case of our spray pyrolysis deposited thin films an increase of 5% in lattice constant for $\Delta T = 780^\circ\text{C}$ is observed. The order of magnitude lattice constant growth within a given temperature interval of the spray pyrolysis film when compared to powders from soft chemical method^[41] can be ascribed to different organic precursors used in preparation of the ceria. The free volume of these films, i.e., the driving force for crystallization therefore is rather larger.

2.2. Non-isothermal Crystallization and Grain Growth of CeO₂ Spray Pyrolysis Thin Films

Mass loss and crystallization was monitored by the TG and DSC signal of as-deposited CeO₂ films that have previously been scratched off from their substrates, Figure 3. Upon heating, a pronounced endotherm with a maxima shifting from 90 to 120°C with increasing heating rate occurs. This is accompanied by a mass loss of 4 wt %, which is assigned to the desorption of water. The mass loss continues with 1.5 wt % until 530°C and remains unaffected by the heating rate. Mass spectrometry revealed that this is due to outgassing water and carbon, residues of the organic precursor solvents used during the spray pyrolysis process. Between 400 and 1000°C there is a broad exotherm resulting from the heat release during crystallization of the sample. In general, an exothermic DSC heat release due to crystallization reflects the transformation of amorphous into crystalline phase and is proportional to the crystallization enthalpy of the material,^[13] Figure 4. The crystallization enthalpy, ΔH_{cryst} , and crystallization peak temperature, T_p , both increase with increasing heating rate for these CeO₂ sprayed thin films, Figure 4a. The crystallized fractions were resolved with respect to temperature and heating rate by integral fractions of the exotherm representing the crystallization enthalpy, Figure 4b. In the crystallized fraction versus temperature plot a typical sigmoidal JMA curve shape similar to classical literature on glass-ceramics is obtained.^[14] Two remarkable occurrences have to be emphasized: When depositing films at substrate temperatures around 390°C , films are amorphous and a temperature increase of only 10°C is required to start crystallization of the films. Secondly, the nucleation phase, indicated by the nonlinear correlation between the crystallized fraction and temperature around 400 – 460°C , proceeds within a very short temperature interval. Whereas crystallization indicated by the linear correlation between crystallized fraction and temperature proceeds over a wide temperature range of $\Delta T = 600^\circ\text{C}$. Compared to a classical glass-ceramic, these precipitation-based thin films show unusual nucleation and crystallization behavior characterized by a short nucleation time briefly above deposition temperature and a wide crystallization temperature regime.

Crystallization enthalpies of $\Delta H_{\text{cryst}} = 93$ – 110 J g^{-1} and crystallization peak temperatures of 543 – 588°C were determined, Figure 5. By the Arrhenius plot of the Kissinger equation^[16]

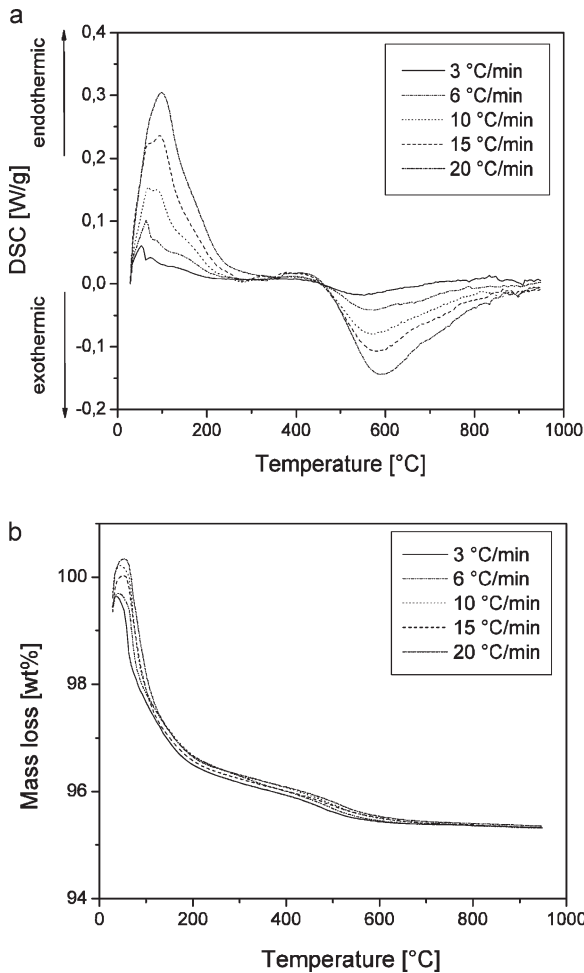


Figure 3. Non-isothermal DSC and TG of CeO₂ produced by spray pyrolysis: a) DSC and b) TG.

shown in Figure 6 an activation energy for the thermally activated crystallization (Q_{cryst}) can be calculated:

$$\ln\left(\frac{T_p^2}{\alpha}\right) = \frac{Q_{\text{cryst}}}{RT_p^2} + \text{const} \quad (1)$$

where R is the gas constant. The activation energy for crystallization is 2.2 eV for CeO₂ spray pyrolysis thin films in static air atmosphere. The present activation energy is comparable to the slightly higher activation energies of 2.4–3.5 eV reported for 8 mol % yttria-doped zirconia produced by precipitation^[9,10] and the lower one for gel derived 3 mol % yttria-doped zirconia of 0.6–1.3 eV.^[15] This difference clearly indicates that the present activation energy of a metal oxide is not only determined by the present inorganic material, but is also influenced by hydrolysis and organics used in preparation.^[9,11,15,42,43] Comparison to classical glass ceramics reveals activation energies of crystallization in equal order of magnitude.^[44]

The non-isothermal grain growth of as-deposited spray pyrolysis thin films with respect to heating rate and temperature

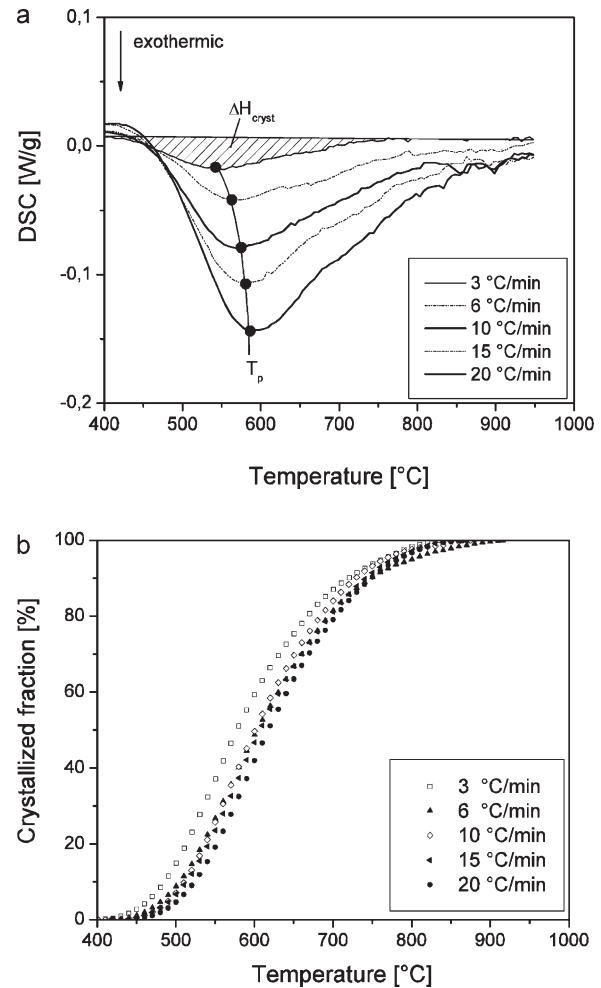


Figure 4. Non-isothermal crystallization of CeO₂ produced by spray pyrolysis: a) exothermic DSC heat release attributed to crystallization and b) its corresponding crystallized fraction. Crystallization enthalpy is denoted as ΔH_{cryst} and crystallization peak temperature as T_p .

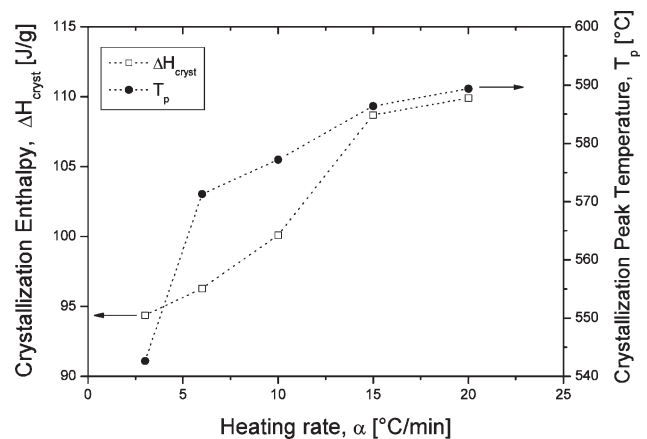


Figure 5. Non-isothermal crystallization enthalpy ΔH_{cryst} and crystallization peak temperature T_p for CeO₂ produced by spray pyrolysis.

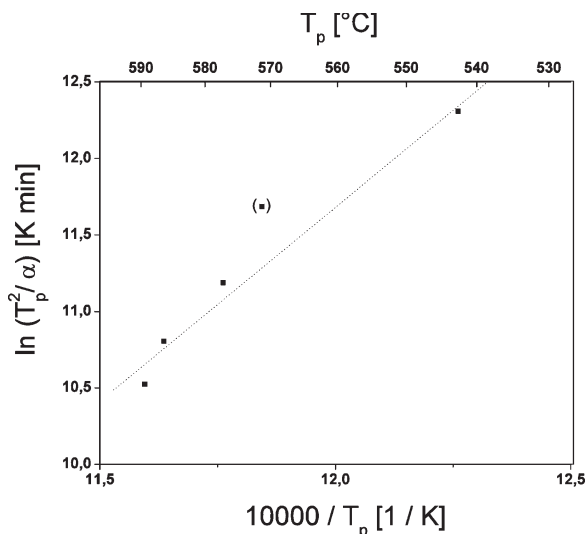


Figure 6. Kissinger plot for CeO₂ produced by spray pyrolysis. Crystallization peak temperature is denoted as T_p and heating rate as α .

is displayed in Figure 7. Average grain sizes have been determined by the XRD line broadening of Bragg peaks measured with in situ heating. Final grain sizes increase with decreasing heating rate. It is interesting to note that the films deposited at 390 °C already have grains in the range of 10 nm within the mainly amorphous matrix. This might also explain the sudden crystallization starting at 400 °C, Figure 4, only 10 °C higher than the deposition temperature.

The crystallized fraction in the films is plotted versus the log of the average grain size for different heating rates in Figure 8. When the crystallized fraction is less than 70%, the crystallized fractions versus average grain size follows a linear behavior with a slope of 1/3 independent of heating rate. This reveals that a kinetically independent process prevails for non-isothermal grain growth of spray pyrolysis CeO₂ thin films. The dependent parameter in non-

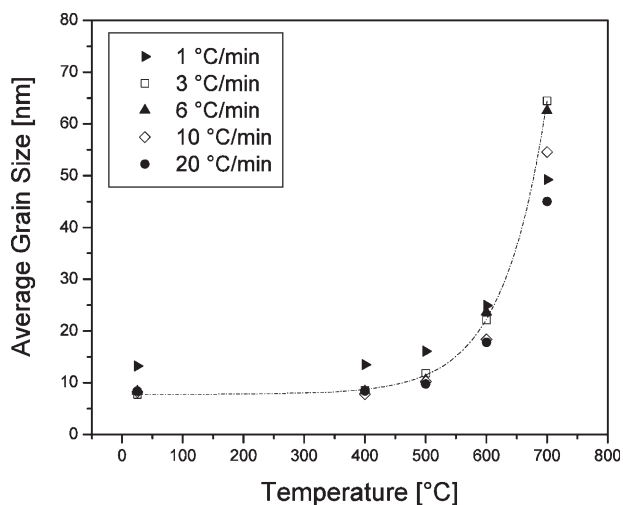


Figure 7. Non-isothermal average grain size measured by in situ XRD from line broadening of spray pyrolysis CeO₂ thin films on sapphire.

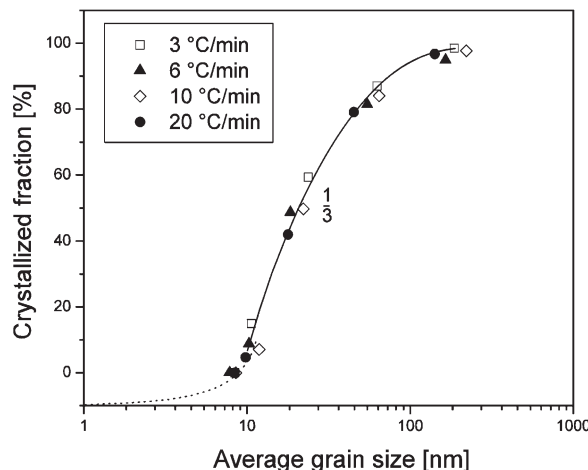


Figure 8. Non-isothermal crystallization versus grain growth of spray pyrolysis CeO₂ thin films.

isothermal grain growth is the transformation of amorphous into crystalline phase, where the volume fraction of crystallized material is proportional to the cube of the average grain size. This means all grains grow independent of each other freely in the amorphous phase. It can be concluded that the dominating driving force for non-isothermal grain growth is the reduction of the free volumetric enthalpy by transformation of amorphous into crystalline phase similar to glass-ceramics or metallic-glasses.^[45,46] For crystallized fractions larger than 70% a deviation from the straight line is present, which holds up to full crystallinity. Here, the grains grow larger than the amorphous phase that is consumed, the grains start to touch each other and classical Ostwald ripening controlled by solid–solid interface reactions prevails. This grain growth mechanism corresponds to classical fully crystalline ceramics where the driving force for grain coarsening is the reduction of its free surface energy.^[47,48]

Two totally different experimental approaches—DSC for crystallized volume fraction and XRD for average grain size—led to these findings. It is interesting to note that although some of the ceria thin films show average grain sizes of 50 nm, films remain in the biphasic amorphous–crystalline state with even up to 50% remaining amorphous phase.

2.3. Isothermal Crystallization and Grain Growth of CeO₂ Spray Pyrolysis Thin Films

Isothermal grain growth data as determined from the in situ XRD analysis of CeO₂ spray pyrolysis thin films are shown in Figure 9. Grain growth occurs mostly in the first 5–10 h of isothermal hold until a stable average grain size is established, at which time grain growth stops. This self-limited grain growth was reported in an earlier study on the grain growth of doped-ceria thin films,^[18] and can be described by a relaxation function:

$$G - G_0 = (G_L - G_0) \left(1 - \exp^{-\frac{t}{\tau}}\right) \quad (2)$$

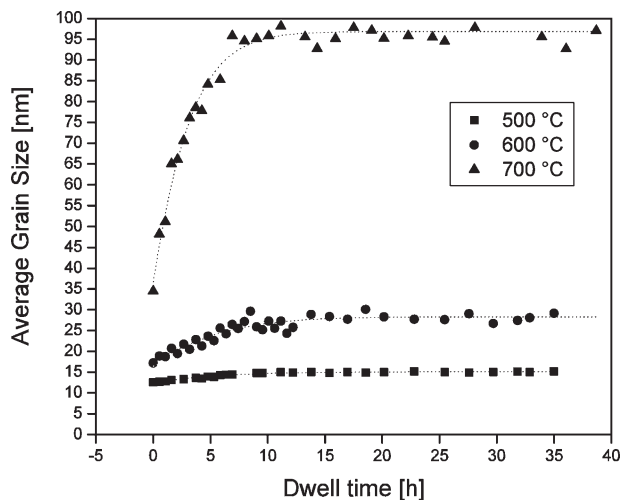


Figure 9. Isothermal grain growth of spray pyrolysis CeO₂ thin films on sapphire. For each isothermal dwell temperature one sample was chosen.

where the limited grain size G_L is the grain size reached after the relaxation time τ , with the average grain size G and the initial grain size G_0 of an isothermal dwell. The diffusion coefficient, D_i , have been determined as a function of isothermal dwell temperature according to ref. [18]:

$$D_i = \frac{(G_L - G_0)^2}{4\tau} \alpha \left(-\frac{Q_{\text{diff}}}{k_B T} \right) \quad (3)$$

where G_L is the limited grain size at which grain growth ceases, G_0 the starting grain size at isothermal dwell time $t=0$, τ the relaxation time, Q_{diff} is the activation energy of diffusion, and k_B is the Boltzmann constant. In Table 2 the relaxation times and diffusion coefficients are presented with respect to isothermal dwell temperature. Increasing the isothermal dwell temperature of CeO₂ sprayed films decreases the relaxation time of grain growth until a stable microstructure is reached. This qualitative observation is in accordance with previous results on self-limited grain growth of Ce_{0.8}Gd_{0.2}O_{1.9-x} sprayed films.^[18] The activation energy of diffusion of CeO₂ sprayed films is low at 0.7 eV and is attributed to surface and interface diffusion processes. Since, volume diffusion would require much higher activation energies above 5 eV, mainly interface diffusion can be attributed for grain coarsening.^[49]

Nucleation characteristics of as-deposited CeO₂ were studied by DSC in a state-of-the-art glass-ceramic isothermal nucleation experiment as shown in Figure 10. In common glass-ceramics or

Table 2. Grain growth relaxation time, τ , and diffusion coefficient, D_i , as a function of isothermal dwell temperature for CeO₂ spray pyrolysis thin films.

Temperature [°C]	Relaxation time, τ [h]	Diffusion coefficient, D_i [m ² s ⁻¹]
500	5.9	9.2e ⁻²⁰
600	5.3	5.5e ⁻²¹
700	3.6	1.5e ⁻²³

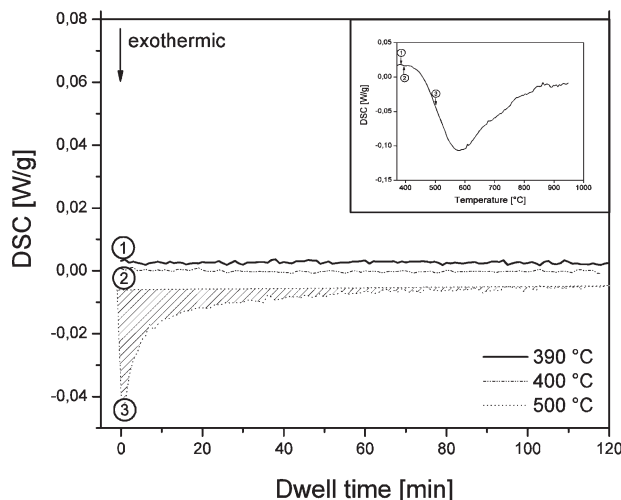


Figure 10. Isothermal nucleation experiment for CeO₂ produced by spray pyrolysis. Exothermic DSC heat release attributed to crystallization during isothermal dwell at temperatures 390–500 °C. Isothermal dwell temperatures were chosen from the non-isothermal dwell experiment with 15 °C min⁻¹ (inset), that during the first heat up to the future dwell temperature for sample 1 (390 °C) crystallization was not activated, for sample 2 (400 °C) crystallization is about to start and for sample 3 (500 °C) crystallization already started.

metallic glasses nucleation can be activated in such isothermal hold experiments at temperatures below those at which the crystallization starts in the non-isothermal annealing. Our samples were heated in accordance to the non-isothermal crystallization results, inset in Figure 10, to three dwell temperatures: before and close to be activated, and finally activated. These temperatures are designated in the inset of Figure 10. At each of these chosen dwell temperatures a sample was held for at least 2 h. In cases where the dwell temperature is below or even close (390–400 °C) to the crystallization starting temperature indicated from a non-isothermal dwell (410–420 °C) the DSC signal remains unaffected by dwell time, Figure 10. The sprayed CeO₂ films show no ability to induce nucleation and crystallize for temperatures below or even close to non-isothermal crystallization starting temperature. This is surprising, since nuclei are present in these films in form of grains smaller than 10 nm in the amorphous matrix, Figure 7. Where the dwell temperature is chosen to be above the non-isothermal activation temperature for crystallization the remaining enthalpy can be determined over dwell time.

The JMA kinetics have been studied via enthalpy determination over the integral of the DSC signal after isothermal holds between 0 and 20 h at 500 °C, Figure 11. Isothermal dwell times were chosen in accordance with previously recorded self-limited grain growth for equal hold temperatures, inset in Figure 11. With the increase in dwell time from 0 to 20 h the integral of the DSC signal decreases drastically until it becomes zero for 20 h of dwell. Since, the remaining crystallization enthalpy is equal to this integral it can be concluded that the crystallization enthalpy is equal to zero for 20 h of dwell and the amorphous-to-crystalline transition is finished at this state. Comparison to grain growth data (inset in Fig. 11) reveals that the amorphous-to-crystalline transition of CeO₂ sprayed films

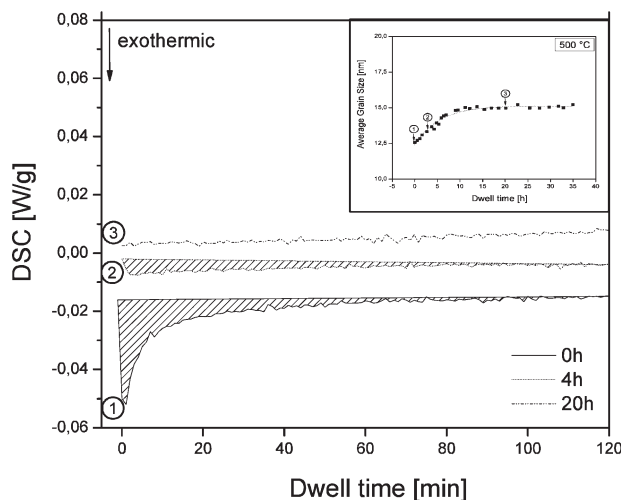


Figure 11. Isothermal crystallization and grain growth experiment for CeO₂ produced by spray pyrolysis at 500 °C. Isothermal dwell times were chosen for the DSC heat release crystallization experiments in accordance to previous isothermal grain growth experiment (inset). Dwell times were chosen as follows that for sample 1 no isothermal grain growth started, sample 2 isothermal grain growth is active and sample 3 grain growth ceased.

occurs in parallel to self-limited grain growth. Once the phase transition is finished for an isothermal dwell, the grain growth ceases and a stable crystalline microstructure is established. The calculated crystallization enthalpies from Figure 11 are displayed for the dwell at 500 °C in Figure 12. These data have been corrected for the 5 vol % crystallization during the non-isothermal heat up between 400 and 500 °C with 15 °C min⁻¹. An initial crystallization enthalpy of 21 J g⁻¹ for 500 °C is freed for no dwell. Increasing the dwell time leads to a rapid decrease to 25% of its initial value within the first 30 min of isothermal hold. Even though a drastic decrease in crystallization enthalpy takes place, an enthalpy of 3 J g⁻¹ is still measurable for 4 h of dwell versus zero for longer dwells. The

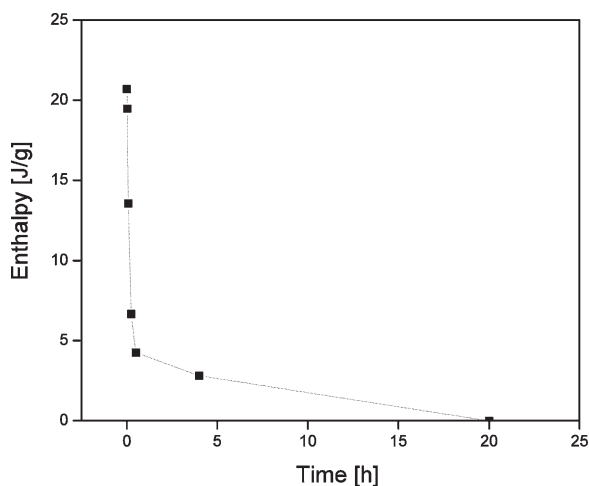


Figure 12. Isothermal test-crystallization enthalpy for CeO₂ produced by spray pyrolysis annealed at 500 °C.

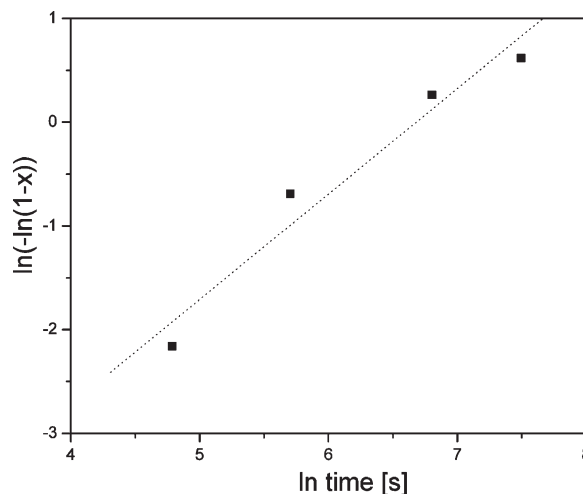


Figure 13. Isothermal JMA analysis of spray pyrolysis CeO₂ thin films for 500 °C.

driving force for the amorphous-to-crystalline transition is nonzero during grain coarsening of self-limited grain growth of CeO₂ sprayed films. Once the transformation is finished, and a purely crystalline phase is present, the crystallization enthalpy approaches zero and grain growth stops.

In the JMA equation, the crystallized fraction x , reaction rate k , dwell time t , and the JMA exponent n are implicated:^[50,51]

$$x(t) = 1 - \exp(-(kt)^n) \quad (4)$$

The JMA exponent n gives an indication of the active nucleation and grain growth processes of a material during an isothermal dwell. From the slope in the $\ln(-\ln(1-x))$ versus $\ln t$ plot the JMA an exponent $n = 1.01$ was determined for CeO₂ sprayed films dwelled at 500 °C, Figure 13.

According to literature a JMA exponent close to 1 is due to a nucleation rate equal to zero and proceeding 3D grain growth in a material.^[52] This interpretation is in agreement with the findings from non-isothermal DSC heating, Figure 4, where only a short nucleation period for $T < 500$ °C was found, and from isothermal grain growth at 500 °C, Figure 9, where grain growth is still active within the time spans studied here for JMA evaluation. Similar findings—JMA exponent close to 1—were reported earlier for the diffusion controlled crystallization of Sr–Bi–Ta-perovskites from an amorphous metal oxide with decreasing and low nucleation rate.^[53] Since crystallization studies on metal oxides and especially isothermal JMA kinetic evaluations are still scarces, the comparison of present isothermal findings for ceria to other metal oxides is not possible.

Figure 14a shows the micrographs resulting from high-resolution TEM (HRTEM). In several different areas of the sample heated for 0 h at 500 °C amorphous material was present, and this is highlighted in the figure. In comparison, the sample heated for 20 h showed larger crystallite sizes and very little or even no amorphous material. The crystallites in the 0 h sample were about 5–7 nm in maximum diameter, while those in the 20 h

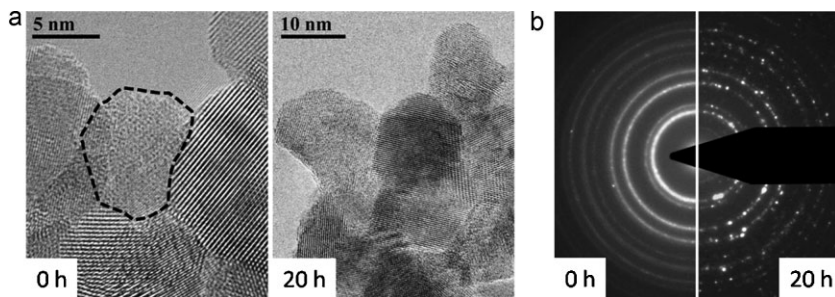


Figure 14. a) TEM bright field images of CeO₂ produced by spray pyrolysis isothermally dwelled for 0 and 20 h at 500 °C. b) Corresponding TEM electron diffraction patterns for 0 and 20 h dwell.

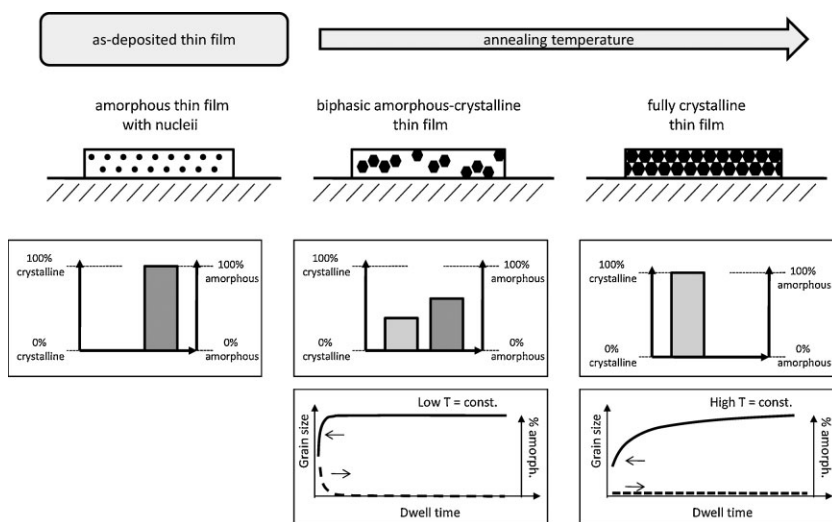


Figure 15. General model for crystallization and grain growth of an amorphous one-phase metal oxide precipitation-based thin film.

sample were routinely larger than 10 nm. The HRTEM observations are confirmed by the selected area electron diffraction (SAED) patterns, shown in Figure 14b. Here, it is apparent that the diffraction rings of the 0 h sample are more continuous than the spotty pattern of the 20 h sample, indicating that the crystallites in the former case are significantly smaller than those in the latter. Furthermore, there is diffuse scattering in the background of the 0 h sample, while no halo is seen in the 20 h sample; such a diffuse signal is indicative of amorphous material.

The TEM results support the DSC findings that once a stable microstructure is reached for these films with respect to dwell time during self-limited grain growth, the material is fully crystalline and no DSC measured enthalpy of transformation can be detected any more.

3. General Model for Crystallization and Grain Growth Kinetics of Metal Oxide Thin Films Deposited by Precipitation

A general model for the crystallization and grain growth kinetics of originally amorphous metal oxides with one kind of cation and

organic solvent is described in Figure 15. After preparation by a precipitation method the metal oxide thin film is in a fully amorphous state with loosely packed cation–oxygen and probably also carbon–oxygen–cation bonds. Only a short temperature increase above the original processing temperature leads to a sudden and short nucleation. The reason for this sharp and strong event is in the nature of these precipitation-based metal oxides where remaining organic impurities can easily act as nucleation sites. Crystallization starts, packing density increases as the bonds become shorter and self-limited grain growth is activated in parallel. In this biphasic amorphous–nanocrystalline state the driving force for the grain growth kinetics is the transformation of the amorphous into a crystalline phase, and thus, reduction of free volumetric enthalpy of the metal oxide. Self-limited grain growth kinetics are observable, where stable grain sizes are established after short isothermal holds once the measurable crystallization enthalpy becomes zero and the metal oxide has transformed to fully crystalline. For heating of the original amorphous metal oxides above the temperature where non-isothermal crystallization is finished, fully crystalline metal oxides remain and typical parabolic grain growth kinetics driven by the curvature of neighboring grains prevail.

4. Conclusions

General rules for the kinetics involved in crystallization and grain growth of a metal oxide, here CeO₂, were investigated as a case study for amorphous ceria produced by precipitation. Thin films were produced with only one kind of cation and organic solvent to avoid the influence of dopants and unpredictable influence of too many organics on crystallization and grain growth via spray pyrolysis. Just above the processing temperature the as-prepared metal oxide transforms from amorphous into a crystalline phase. The driving force for grain growth is the reduction of free volume and crystallization enthalpy during an isothermal hold for these biphasic amorphous–crystalline metal oxides. Once the crystallization enthalpy equals zero, stable microstructures are established, and grain growth ceases. Self-limited grain growth kinetics prevail for the biphasic ceramics with up to 70–80 vol % crystallized material. Increasing the temperature above the crystallization temperature leads to fully crystalline microstructures. State-of-the-art parabolic grain growth determined by the grain curvature of neighboring grains holds then for fully crystalline ceramics.

This knowledge can be taken as a base for microstructure engineering of originally amorphous metal oxide thin films made via precipitation for devices-based on MEMS technology such as, i.e., dye-solar cells where organics are involved in preparation and the functionality of the solar cell films^[54] or resistive-sensors where

the sensor response and sensitivity is strongly dependent on crystallinity degree of resistive layer.^[55]

The kinetics of nucleation, crystallization, and grain growth characteristic of CeO₂ were measured for thin films prepared on the base of a tetrathylene glycole spray pyrolysis precursor:

1. Nucleation can be induced with a 10 °C temperature increase above the original deposition temperature of 390 °C. However, it cannot be induced for hold temperatures lower or close to the non-isothermal crystallization starting temperature. Further, no glass-transition temperature is measurable. These two nucleation characteristics differ substantially from classical glass-ceramics.
2. Crystallization prevails over a wide temperature range of $\Delta T = 600$ °C and follows JMA kinetics for the conversion of amorphous into crystalline phase. The crystallographic density increases by roughly 1 g cm⁻³ upon non-isothermal heating to fully crystalline ceria. Typical crystallization enthalpies of 93–110 J g⁻¹ for a heating rate of ± 6 –20 °C min⁻¹ are measurable. The overall non-isothermal activation energy of crystallization is 2.2 eV. The isothermal crystallization experiment for 500 °C revealed that 3D grain growth is active and the nucleation rate is equal to zero. Here, the initial crystallization enthalpy is 21 J g⁻¹ and decreases to zero for 20 h of hold.
3. Grain growth occurs parallel to crystallization for biphasic films. When the crystallized fraction is less than 70%, the crystallized fractions versus average grain size follow a linear behavior with a slope of 1/3 independent of the heating rate. Self-limited grain growth kinetics rule for an isothermal dwell of CeO₂; its relaxation time decreases from 5.9 to 2.9 h until a stable grain size is established and full crystallinity is reached for temperatures 500–700 °C. Grain coarsening is controlled by interface diffusion characterized by a low activation energy of 0.7 eV. Diffusion coefficients range from $9.2e^{-20}$ to $1.5e^{-23}$ for 500–700 °C, respectively.
4. Comparison of the present crystallization findings for CeO₂ with literature reveals that the actual enthalpies and temperature ranges of the biphasic state depend highly on the organics used in preparation of a participation method.

5. Experimental

Thin Film Preparation: Ceria spray pyrolysis precursor solutions were made of 0.1 mol l⁻¹ cerium nitrate (Alfa Aesar, 99% purity) dissolved in 10:90 vol % water and tetraethylene glycol (Aldrich, >99% purity). These precursor solutions were fed to a spray gun (Compact 2000 KM, Böhlfach Verfahrenstechnik, Germany) with a liquid flow rate of 5 mL h⁻¹ and atomized with 1 bar air pressure. The droplets produced in this manner were sprayed on a heated sapphire single crystal substrate (Stettler, Switzerland) at 390 ± 5 °C for 1.45 h. The working distance between the spray nozzle and the hot plate was kept at 39 cm during all experiments. The spray pyrolysis process is described in further detail elsewhere [7–9]. After spray pyrolysis film deposition the thin films are amorphous and can be converted to biphasic amorphous-nanocrystalline or totally nanocrystalline films by annealing at temperatures higher than the spray pyrolysis deposition temperature [10,11].

Microstructure: The top-view microstructures of the thin films were characterized using scanning electron microscopy (SEM, Zeiss Leo 1530, Germany). For this the thin films were sputtered (Bal-Tec, SCD 050, Sputter

Coater) with a Pt coating in order to avoid charging and to allow imaging at higher resolutions.

Two samples were prepared for transmission electron microscopy (TEM): one that was heated to 500 °C for 0 h and one that was heated to 500 °C and held for 20 h. Heat treatments of both samples took place in the DSC experimental setup as described later to maintain consistency between the characterization methods. As such, the samples had been scraped off the sapphire substrates and were in powdered form. Some of each powder was mixed into 2 mL of ethanol and sonicated for 10 s to make a suspension. Then, one drop of each suspension was put onto separate Cu TEM grids with holey C films. The TEM investigation was made on a Philips CM 30 microscope operated at 300 kV with a LaB₆ emitter and Super Twin lens.

Chemistry: The chemical compositions of the films were determined by energy dispersive X-ray spectroscopy (EDX, Leo 1530, Germany) using the cerium L-line at 20 kV. For quantitative EDX analysis, the Proza correction method was chosen.

Crystallization: Crystallization of the amorphous spray pyrolysis thin films during annealing was measured in calibrated differential scanning calorimetry (DSC/TG, Netzsch STA 449C) experiments. In these measurements the degree of crystallinity from the exothermic heat loss signal and the amount of amorphous versus crystalline phase can be determined [56]. In order to quantify the DSC results, the instrument was calibrated with calibration standards (Netzsch 6.223.5-91.2) of known melting points and heat losses, or phase changes. Then as-deposited amorphous CeO₂ thin films were scratched off from the sapphire substrate and the powder obtained as such was analyzed in DSC. The powder was always enclosed in a Pt pan with lid and measured against an empty Pt pan with lid as a reference under static air atmosphere.

In the case of continuous heating, 50 ± 1 mg of amorphous CeO₂ powder was measured at heating rates of 1–20 °C min⁻¹. A subsequent correction measurement for quantitative DSC analysis using a totally crystallized CeO₂ spray pyrolysis powder of the same mass at equivalent experimental conditions was performed. The signal of this experiment was recorded and subtracted from the measurement of the originally amorphous powder.

For the isothermal analysis, amorphous CeO₂ spray pyrolysis powder of 35 ± 1 mg was heated with 15 °C min⁻¹ to the target dwell temperature in all experiments. In the case of the isothermal nucleation experiments this signal was directly subtracted by the isothermal dwell of a totally crystalline CeO₂ spray pyrolysis powder. The Johnson–Mehl–Avrami (JMA) experiment for an isothermal hold at 500 °C represented a special kind of isothermal crystallization experiment: For this the amorphous CeO₂ powder was dwelled, cooled to room temperature and subsequently the remaining enthalpy was determined during a hold of 2 h at 500 °C. These measurements were corrected by fully crystallizing the sample with non-isothermal heating to 1000 °C with 15 °C min⁻¹ after the latter heat treatment, and subsequently conducting an isothermal 2 h hold at 500 °C. The subtraction of this latter isothermal result for the fully crystalline state from the original isothermal for the freed enthalpy resulted in the corrected DSC profile of the material.

Grain Growth: Average grain size was determined by X-ray diffraction (XRD, Bruker AXS D8 Advance). The development of line widths of the Bragg peaks during in situ annealing in a furnace (Anton Paar HTK 1200) provided information on the average grain size development. Diffracted X-rays from the sample were detected by a position sensitive detector (Braun PSD ASA-S). The XRD setup was equipped with a copper radiation source ($\lambda = 0.15404$ nm) operated at 40 kV and 40 mA followed by a $K\alpha_1$ -Ge monochromator (Bruker AXS). The average grain size was determined from the full width at half maximum (FWHM), by using Fourier analysis of the XRD peaks, refined by a split Pearson 7 function (Software EVA 6.0). The FWHM results from instrumental broadening and microstructure. The instrumental peak broadening of the diffractometer was determined by measuring a commercially available microcrystalline and stress-free CeO₂ powder of large particles (Alfa Aesar, purity 99.99%). The instrumental broadening can be eliminated from the FWHM using the Warren and Biscoe equation [57]. Average grain size was calculated from according to the Scherrer equation [58,59]. The lattice parameter of the cubic CeO₂

crystal lattice was calculated from the position of the observed diffraction lines in the XRD pattern. The crystallographic density was calculated in accordance with ref. [60].

Received: February 12, 2009
Published online: June 27, 2009

- [1] J. Musil, et al. *Thin Solid Films* **2005**, *475*, 208.
- [2] T. P. Niesen, M. R. De Guire, *Solid State Ionics* **2002**, *151*, 61.
- [3] P. S. Patil, *Mater. Chem. Phys.* **1999**, *59*, 185.
- [4] C. H. Gorbitz, H. P. Hersleth, *Acta Crystallogr., Sec. B: Struct. Sci.* **2000**, *56*, 526.
- [5] P. Van Der Sluis, J. Kroon, *J. Cryst. Growth* **1989**, *97*, 645.
- [6] P. van der Sluis, A. M. F. Hezemans, J. Kroon, *J. Cryst. Growth* **1991**, *108*, 719.
- [7] H. S. Kang, Y. C. Kang, H. Y. Koo, S. H. Ju, D. Y. Kim, S. K. Hong, J. R. Sohn, K. Y. Jung, S. B. Park, *Mater. Sci. Eng. B* **2006**, *127*, 99.
- [8] B. Ksapabutr, E. Gulari, S. Wongkasemjit, *Mater. Chem. Phys.* **2006**, *99*, 318.
- [9] C.-W. Kuo, Y.-H. Lee, I. M. Hung, M.-C. Wang, S.-B. Wen, K.-Z. Fung, C.-J. Shih, *J. Alloys Compd* in press.
- [10] S. Ramanathan, *J. Am. Ceram. Soc.* **1995**, *78*, 429.
- [11] J. Tartaj, J. F. Fernandez, C. Moure, P. Duran, *Mater. Res. Bull.* **1997**, *32*, 1525.
- [12] J. Livage, K. Doi, C. Mazieres, *J. Am. Ceram. Soc.* **1968**, *51*, 349.
- [13] M. M. R. Boutz, R. Scholtenhuis, A. J. A. Winnubst, A. J. Burggraaf, *Mater. Res. Bull.* **1994**, *29*, 31.
- [14] A. Aronne, A. Marotta, P. Pernice, M. Catauro, *Thermochim. Acta* **1996**, *275*, 75.
- [15] J. Malek, S. Matsuda, A. Watanabe, T. Ikegami, T. Mitsushashi, *Thermochim. Acta* **1995**, *267*, 181.
- [16] J. L. M. Rupp, T. Drobek, A. Rossi, L. J. Gauckler, unpublished.
- [17] J. L. M. Rupp, C. Solenthaler, P. Gasser, U. P. Muecke, L. J. Gauckler, *Acta Mater.* in press.
- [18] J. L. M. Rupp, A. Infortuna, L. J. Gauckler, *Acta Mater.* **2006**, *54*, 1721.
- [19] I. Kosacki, T. Suzuki, V. Petrovsky, H. U. Anderson, *Solid State Ionics* **2000**, *136*, 1225.
- [20] I. Kosacki, T. Suzuki, H. U. Anderson, P. Colomban, *Solid State Ionics* **2002**, *149*, 99.
- [21] T. Suzuki, I. Kosacki, H. U. Anderson, P. Colomban, *J. Am. Ceram. Soc.* **2001**, *84*, 2007.
- [22] J. L. M. Rupp, L. J. Gauckler, *Solid State Ionics* **2006**, *177*, 2513.
- [23] T. Suzuki, I. Kosacki, H. U. Anderson, *Solid State Ionics* **2002**, *151*, 111.
- [24] J. L. M. Rupp, A. Infortuna, L. J. Gauckler, *J. Am. Ceram. Soc.* **2007**, *90*, 1792.
- [25] T. S. Stefanik, H. L. Tuller, *J. Eur. Ceram. Soc.* **2001**, *21*, 1967.
- [26] I. Kosacki, H. U. Anderson, *Sens. Actuators, B: Chem.* **1998**, *48*, 263.
- [27] P. Jasinski, T. Suzuki, H. U. Anderson, *Sens. Actuators, B: Chem.* in press.
- [28] H.-J. Beie, A. Gnorich, *Sens. Actuators, B: Chem.* **1991**, *4*, 393.
- [29] A. Bieberle-Hütter, D. Beckel, U. P. Muecke, J. L. M. Rupp, A. Infortuna, L. J. Gauckler, *MST News* **2005**, *4*, 12.
- [30] U. P. Muecke, D. Beckel, A. Bernard, A. Bieberle-Hütter, S. Graf, A. Infortuna, J. L. M. Rupp, J. Schneider, P. Müller, J. Gauckler, unpublished.
- [31] D. Beckel, A. Bieberle-Hütter, A. Harvey, A. Infortuna, U. P. Muecke, M. Prestat, J. L. M. Rupp, L. J. Gauckler, *J. Power Sources* **2007**, *173*, 325.
- [32] A. Bieberle-Hütter, D. Beckel, A. Infortuna, U. P. Muecke, J. L. M. Rupp, L. J. Gauckler, S. Rey-Mermet, P. Murali, N. R. Bieri, N. Hotz, M. J. Stutz, D. Poulikakos, P. Heeb, P. Muller, A. Bernard, R. Gmur, T. Hocker, *J. Power Sources* **2008**, *177*, 123.
- [33] U. P. Muecke, K. Akiba, A. Infortuna, T. Salkus, N. V. Stus, L. J. Gauckler, *Solid State Ionics* **2008**, *178*, 1762.
- [34] L. J. Gauckler, D. Beckel, B. E. Buegler, E. Jud, U. P. Mücke, M. Prestat, J. L. M. Rupp, J. Richter, *Chimia* **2004**, *58*, 837.
- [35] P. Palmisano, N. Russo, P. Fino, D. Fino, C. Badini, *Appl. Catal., B: Environ.* **2006**, *69*, 85.
- [36] Z.-Y. Yuan, V. Idakiev, A. Vantomme, T. Tabakova, T.-Z. Ren, B.-L. Su, *Catal. Today* **2008**, *131*, 203.
- [37] M. Thammachart, V. Meeyoo, T. Risksomboon, S. Osuwan, *Catal. Today* **2001**, *68*, 53.
- [38] M. Das, S. Patil, N. Bhargava, J.-F. Kang, L. M. Riedel, S. Seal, J. J. Hickman, *Biomaterials* **2007**, *28*, 1918.
- [39] M. Mogensen, N. M. Sammes, G. A. Tompsett, *Solid State Ionics* **2000**, *129*, 63.
- [40] H. Nitani, T. Nakagawa, M. Yamanouchi, T. Osuki, M. Yuya, T. A. Yamamoto, *Mater. Lett.* **2004**, *58*, 2076.
- [41] M. Kamruddin, P. K. Ajikumar, R. Nithya, A. K. Tyagi, B. Raj, *Scr. Mater.* **2004**, *50*, 417.
- [42] P. Duran, J. Tartaj, J. F. Fernandez, M. Villegas, C. Moure, *Ceram. Int.* **1999**, *25*, 125.
- [43] P. Duran, J. Tartaj, J. F. Fernandez, C. Moure, *Mater. Lett.* **1998**, *36*, 174.
- [44] M. A. Lamkin, F. L. Riley, R. J. Fordham, *J. Eur. Ceram. Soc.* **1992**, *10*, 347.
- [45] H. V. Atkinson, *Acta Metall.* **1988**, *36*, 469.
- [46] I. Gutzow, J. Schmelzer, *The Vitreous State: Thermodynamics, Structure, Rheology, and Crystallization: Chapter 7: Catalyzed Crystallization of Glass-Forming Melts*, Springer-Verlag, Heidelberg **1995**, pp. 302–305.
- [47] J. E. Burke, E. Turnbull, *Prog. Metal Phys.* **1952**, *3*, 220.
- [48] J. E. Burke, *Trans. Am. Inst. Mining Metall. Eng.* **1949**, *180*, 73.
- [49] T. S. Zhang, J. Ma, L. B. Kong, Z. Q. Zeng, P. Hing, J. A. Kilner, *Mater. Sci. Eng. B* **2003**, *103*, 177.
- [50] M. Avrami, *J. Chem. Phys.* **1941**, *9*, 177.
- [51] M. Avrami, *J. Chem. Phys.* **1939**, *7*, 1103.
- [52] K. A. Jackson, *Kinetic Processes*, Wiley-VCH, Weinheim, Germany **2004**, chapter 15.
- [53] W.-C. Kwak, Y.-M. Sung, *J. Eur. Cer. Soc.* **2004**, *24*, 1603.
- [54] M. Grätzel, *Inorg. Chem.* **2005**, *44*, 6841.
- [55] G. Sberveglieri, *Sens. Actuators* **1995**, *23*, 103.
- [56] C. Michaelsen, M. Dahms, *Thermochim. Acta* **1996**, *288*, 9.
- [57] C. N. J. Wagner, E. N. Aqua, *J. Less Common Metals* **1965**, *8*, 51.
- [58] P. Scherrer, *Mathematisch-physikalische Klasse* **1918**, *1*, 98.
- [59] A. J. C. Wilson, *X-ray Optics*, **1949**, p. 5.
- [60] W. Kleber, H.-J. Bausch, J. Bohm, *Einführung in die Kristallographie: Chapter 3: Physikalisch-chemische Kristallographie*, **1998**, pp. 200–204.